Understanding mechanisms of drying of a cellulose slurry by Magnetic Resonance Imaging

N. Ben Abdelouahab[1,2], A. Gossard[2], X. Ma[1], H. Dialla[1,2], B. Maillet[1], S. Rodts[1], P. Coussot[1]

[1] Lab. Navier, Ecole des Ponts, Univ Gustave Eiffel, CNRS, 77420, Champs sur Marne, France
[2]CEA, DES, ISEC, DMRC, Univ Montpellier, Marcoule, France

Abstract: This study concerns the spatial evolution of the internal components of a macroscopic sample of cellulose slurry during its convective drying. In a first stage, some water is extracted which induces a shrinkage of the structure, the sample remaining saturated, i.e. the solid porous structure made of fibers in contact remains filled with water. In a second stage, when capillary effects are unable to induce further shrinkage, the porous structure formed by the cellulose network homogeneously desaturates and all bulk water is extracted. All along these two stages the drying rate remains constant. Confined water (i.e. likely between macrofibrils) and possibly bound water start to be extracted in a third final stage, during which the sample somewhat further shrinks. In that case a dry front tends to develop from the free surface of the sample, but the water content still decreases homogeneously in the wet region, which suggests that a connected hydraulic network for the confined and bound water persists. This network in fact already ensured the full extraction of bulk water at the end of the second stage keeping a constant drying rate, in contrast with simple porous media.

Introduction

Water-cellulose suspensions, pastes or slurries, are dried at various steps of industrial processes (Hubbe et al. 2007, Sinquefield et al. 2020) or when they are used as poultices for salt removal from ancient walls (Vergès-Belmin et al. 2011). The best technique for water removal through drying is the object of intense research (Posada et al. 2020, Peng et al. 2012, Lovikka et al. 2016), in particular to avoid hornification or other mechanisms by which the local structure is affected by drying (Hubbe et al. 2017, Beaumont et al. 2017, Weise et al. 1996). The evolution of the porous structure and/or the pore size distribution, considering both free and bound water, has also been studied by NMR (Nuclear Magnetic Resonance) (Häggkvist et al. 1998, Topgaard and Söderman 2002) and DSC (Differential Scanning Calorimetry) (Park et al. 2006). In this context, Topgaard and Söderman (2002) showed that three types of water disappear successively, first bulk water, then water in pores with at least one dimension on the micron scale, and finally water in nanometric pores. These three types of water might correspond respectively to the bulk water, the “freezing bound water”, and the non-freezing bound water, identified by DSC (Weise et al. 1996).

We emphasize that in previous studies the possible spatial heterogeneity of the system, i.e. the development of regions with different water contents, and possibly water types, inside the sample, has generally been neglected. Yet, this is a critical question as soon as one considers the drying of a porous medium, since the extraction of water from the interior of the sample is induced by evaporation resulting from a gradient of RH (relative humidity) between the sample surface and the ambient air. Under these conditions, it would not be surprising that a gradient of water content develops inside the medium. On another side, the different regimes of drying depend on the processes at the origin of water transport and extraction, which can inform on the cellulose structure, water types and exchanges inside the medium.

Thus, it is useful to appreciate the way a cellulose slurry dries and look at the internal distribution of water content in time, the distribution of water types, the mechanism of water transport, and the possible shrinkage of the structure.

The mechanisms of drying of non-deformable, homogeneous porous structures initially filled with a liquid (perfectly wetting the solid) and submitted to a constant air flux along one of its external surface usually follows a well admitted scenario (Van Brakel 1980, Prat 1993, Coussot 2000, Tsimpanogiannis et al. 1999, Lehmann et al. 2008, Shokri et al. 2009, Yiotis et al. 2012). During a long first period, the drying rate remains constant and the saturation (i.e. the liquid to pore volume ratio) decreases homogeneously in the sample. This regime is capillary-driven, i.e. any withdrawing of liquid leads to a homogeneous redistribution of the liquid throughout the sample due to capillary effects. This maintains a sufficient density of small liquid patches around the sample free surface, which keeps approximately constant the boundary conditions in terms of vapor field in this region, which in turn induces a constant drying rate. In the next regime, i.e. when the liquid film size is too thin or, equivalently, the external evaporation rate is too large, capillary effects are unable to re-equilibrate sufficiently rapidly the liquid network, which tends to induce a complete drying of some region situated below the free surface. For model porous systems, such a scheme remains qualitatively valid down to nanometric pore size (Thiery et al. 2017).

With a cellulose slurry, there is first a major complication regarding this scheme: the elements composing the structure, i.e. the cellulose fibers, can deform when submitted to some stress such as the capillary stresses which typically develop during drying; as a consequence the apparent volume of the solid structure of the porous medium may vary, so that we are dealing with a compressible porous medium. In that case, some water content gradient can develop, as was for example observed for emulsions (Goavec et al. 2018), microgels (Keita et al. 2016 a) or polymeric bi-porous media (Lerouge et al. 2020).

Here we study a relatively thick cellulose slurry sample initially containing a relatively small volume fraction of cellulose, and we follow its characteristics by NMR and MRI (Magnetic Resonance Imaging) all along its drying process. The data analysis provides a full scheme of the mechanisms at work during drying of such a material. We start by presenting the materials and procedures (Section II), then we present the results (Section III) and finally we discuss these data (Section IV).

Materials and procedures

Material

The cellulose paste was prepared as follows: cellulose fibers (Arbocel® BC1000, supplied by *Kremer Pigmente)*, were mixed (at a weight solid fraction of 7%) with distilled water at room temperature for twenty minutes until obtaining a homogeneous paste. Arbocel® BC1000 is composed of natural crystalline cellulose fibers (with 99.5% cellulose content), of hydrophilic nature, which is only partly swollen by water without dissolving and is insoluble in most solvents. The average fiber thickness and length are respectively about 20 µm and 700 µm (see Fig. 1). The fiber density is $1500\mathrm{kg\,m^{-3}}$. It follows that the initial volume fraction of the cellulose in the sample is 5.3%. With such a compressible material of complex porous structure, we can appreciate the porous structure and estimate the pore size from a view of the compressed fiber packing after the paste shrinkage due to drying (see Fig. 1). In that case the typical pore size is a few tens of microns, and we can expect that the effective pore size at the beginning of the test is slightly larger. The drying of a cellulose paste was also observed using

Environmental Scanning Electron Microscopy (ESEM). The experiment was performed on a FEI QUANTA 200 ESEM FEG device. The temperature in the ESEM chamber was fixed at 5°C and the vapor pressure and the relative humidity was varied from 870 Pa to 176 Pa and from 100 % to 20 % respectively.

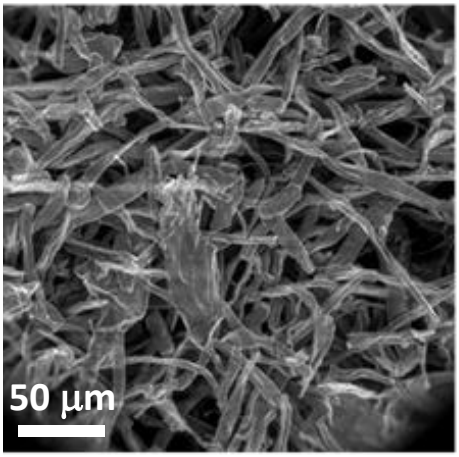

Fig.1: ESEM Image of the cellulose paste microstructure

Set up

The cellulose paste was placed in a cylindrical glass dish ($D = 9cm, H = 5cm$) up to a height of 4 cm. Under these conditions, only the top surface of the paste is in contact with air (see Fig. 1). A small container enclosing water was placed over a tripod lying on the center of the paste. At the very beginning of the test it slightly sinks (see Fig. 3) in the very soft paste, but then it remains at a fixed distance from the free surface of the paste, so that MRI measurements allows to determine the effective position of the free surface above the solid structure of the slurry. We then induce a constant dry air flux (relative humidity below 0.5%) vertically against the sample free surface and we follow the water amount distribution in time with NMR.

NMR

All measurements are performed at a 24/80 DBX 0.5-T ^{1}H MRI spectrometer by Bruker (20 cm open diameter in the sample area), operating at 20MHz. We look at the evolution of the water distribution in time with the help of MRI measurements, either from qualitative 2D images of a sample cross section along the vertical axis, or from quantitative 1D projections of the liquid content on the vertical axis, hereunder referred to as 1D profiles, where each data point represents the integrated NMR signal (proportional to the water mass) in a 1 mm thick layer. During the whole drying process, which usually took 2 weeks, the sample was simply left at the magnetic center of the MRI system and submitted to the dry air flux (see Fig. 2).

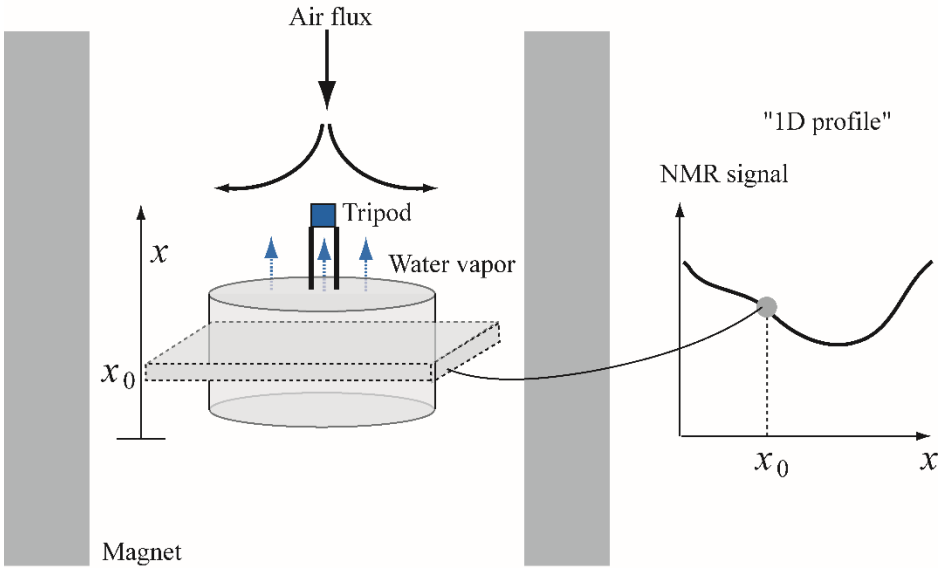

Fig.2: Conceptual scheme of the set up and the 1D MRI profile measurement (one point along the profile corresponds to the total NMR signal in a thin layer of sample)

Profile measurements (1D MRI)

The distribution of apparent water along the sample vertical axis (x) (see Fig. 2) was measured by means of the Single Point Imaging (SPI) sequence (Emid et al. 1985, Bogdan et al. 1995). In addition to other purposes such as removing susceptibility and chemical shift artifacts, this sequence is dedicated for studying materials with very short spin-spin T_2 relaxation times, i.e. shorter than typically 1 ms, in contrast with more classical spin-echo sequences. As a consequence, here this sequence will a priori allows us to follow the water amount in almost any pore type in the system, in particular possible bound water or thin liquid films possibly formed in the ultimate stages of drying.

The detailed parameters of the MRI sequence used were described in a previous study (Ben Abdelouahab et al. 2019). Our implementation allows the recording of a series of MRI profiles (Prado et al. 1997) as a function of time (tau) over some time interval. The different T1 values were estimated from independent measurements with a spectrometer, and the parameters of the sequence (in particular the repetition time) for 1D profiles were adjusted to have a minor influence of T1 over the whole range of water states in the sample. The local NMR signal is then extrapolated based on an exponential model ($s = s_0 \exp(-t/T_2^*)$ in which t is the time and T_2^* the relaxation time) to provide a profile $s_0(x)$ compensated for the effect of spin-spin relaxation and possibly field inhomogeneities. The representation of the signal relaxation with a monoexponential function is an approximation which may be shown to provide a reliable estimate of the amount of water present even in slight multiexponential cases (note that in any event the distribution of T_2^* is in a range of values lower than the T_2 values presented below). We then yield the distribution of water in small cross-section layers (1 mm thickness) along the sample axis (see Fig. 2) at different positions and time. Note that the measured profiles are also sensitive to the geometry of the sample and its container, which can explain the appearance of ramps on the edge of the profiles, i.e., a progressive decrease of the NMR signal over the millimeter order even if the saturation in the sample is homogeneous.

Imaging

2D Images were obtained in a vertical (radial) cross section of the sample by means of a spin-echo sequence with a slice selection (Callaghan 1993). The sequence tuning used a vertical and horizontal (read out) field of views of 6.5 cm and 20 cm respectively, with a space resolution of 1mm in both directions. The slice thickness is 1cm. The whole imaging process was repeated 8 times on purpose of phase cycling and signal accumulation, with *TR*=1 s and *TE*=4.2 ms, and lasted about 9 minutes. The measurements are weighted by spin-spin relaxation so as to well observe the various parts of the sample. The signal intensity on the MRI picture is therefore not directly proportional to the local water amount, but instead reads $s = s_0 \exp(-TE/T_2)$. However, we can remark that the local relaxation time T_2 in a desaturating porous medium decreases with the local water amount (as the liquid volume decreases more rapidly than the area of the liquid interface with air or solid). Indeed, according to the fast exchange Brownstein and Tarr (1977) model the relaxation time essentially varies with the volume/surface ratio. In a desaturating porous medium, air penetrates the liquid network, thus inducing new liquid-air interfaces and forming thinner liquid films along the solid surface, which decreases with the ratio of the volume of liquid in a pore to the wetted surface of this pore. This implies that, in any event, the apparent signal intensity in such images slightly decreases when the water amount decreases, which allows to follow qualitatively the 2D distribution of water in time.

Relaxometry

We also measured the complete NMR relaxation through a Carr-Purcell-Meiboom-Gill (CPMG) sequence composed of a first π/2-pulse and 2000 π-pulses during 5000 ms distributed in logarithmic intervals. The repetition time is 10 s to get a complete relaxation of all protons. This sequence is repeated 24 times to increase the signal to noise ratio**.** The distribution of the relaxation time T_2 is then resolved by means of ILT (Inverse Laplace Transform) with a non-negative least square fit to the data with Tikhonov regularization, similar to the 'Contin' method (Whittall and MacKay 1989, Provencher 1982), and described in more details in Faure and Rodts 2006. We finally get an apparent statistical distribution of T_2, expressed in terms of signal intensity associated with each possible value of T_2. Note that the exact shape of this "T-distribution" depends on the technique of regularization used, and in particular on the value of one specific factor used in the procedure (Faure and Rodts 2006), but the positions of the peaks and the amount of liquid associated with these peaks are robust values.

Roughly speaking the relaxation time is related to the mobility of water molecules, and specific interactions of water with their environment (e.g. adsorption, proton exchange with other species, or magnetic interactions at nanoscale). In the particular case of water embedded in a pore cavity, within the usual hypothesis of biphasic fast exchange (Philippot et al. 1998), the general property is that, for a given pore shape, the relaxation time decreases when the pore size decreases (Korb 2018). As a consequence, if the T-distribution presents some peaks, they indicate different classes of pore sizes and/or water in different "states" (e.g. bound or free water), and the amount of liquid in each class may be estimated from the integral of the T-distribution around the peak.

Compression test

In order to estimate the force needed to compress the solid structure of the sample we placed the dry cellulose in a cylindrical container (diameter: 4 cm, initial height of cellulose: 15 cm) with a piston free to move in the cylinder on its top. The initial cellulose concentration in air was 7%. We then applied an increasing force to the piston, which induced its displacement to a new position. Thus the normal stress could be estimated by dividing the force by the area of the cylinder section, and the corresponding mean concentration of the cellulose sample could be computed from the loss of volume. More precisely the volume fraction of cellulose is equal to the cellulose volume (mass to density ratio) divided by the current sample volume. Note that the data obtained from such a test can only provide

a rough evaluation of the normal stress vs concentration. Indeed, although we expect the shear stress along the (smooth) walls to be low due to wall slip effect we ignore its exact contribution to the measured force. Moreover, the stress and concentration are computed assuming the compression is homogeneous, which might not be strictly the case.

Results

We observe first a decrease of the level of the cellulose paste (see Fig.3 a,b,c,d) with an NMR signal remaining almost constant in the paste volume, while the distance between the small water container and the paste surface remains constant. This means that, during this stage, water is extracted from the paste by evaporation from the free surface and the paste drying induces a homogeneous longitudinal shrinkage. The NMR signal remains approximately constant because the water fraction remains close to 1.

In the next stage the apparent paste volume remains constant, which means that no more contraction occurs, while the NMR signal starts to decrease, first somewhat heterogeneously (see Fig.3 d,e), then homogeneously (see Fig.3 e,f,g). We have no clear explanation for this initial heterogeneity, in particular for the faster desaturation along the cylinder walls. Neglecting this phenomenon, we can consider that during this phase the solid structure of the cellulose paste is kept fixed and the water is extracted homogeneously from this structure. In the last stage (see Fig.3 h,i) a region with no apparent NMR signal develops from the sample top, while some slight contraction occurs (see dashed line in Fig.4).

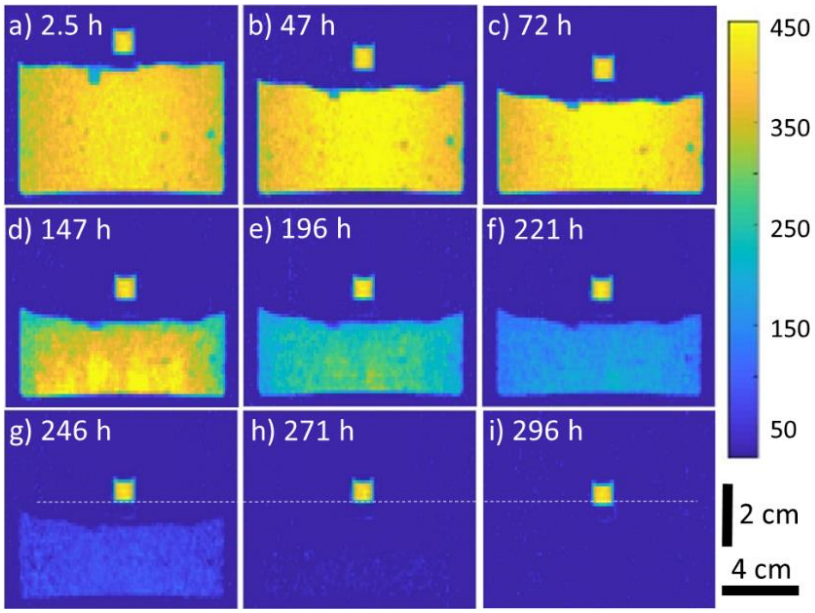

Fig. 3: 2D MR images of the cellulose paste at different times during drying. Note the « tripod » (cubic volume filled with water) lying at a given distance over the sample free surface. The NMR signal on the color scale (in arbitrary units) is for each phase an increasing, but non-linear, function of the local water amount (see Section II)

The quantitative 1D profiles (see Fig.4) evolve in agreement with this description. As drying progresses the total amount of water, corresponding to the integral of the signal over each profile, decreases. We can observe first a shrinking period (up to the dotted line), that we call here Regime A, during which the wet thickness of the sample, i.e. the length of the profile along the abscissa axis in Fig.4, decreases. We here interpret this effect as shrinkage rather than the growth of a dry region starting from the top surface of the sample thanks to the 2D images showing a constant distance between the small water container and the apparent sample top surface (see Fig.3). It may be noticed that despite this shrinkage, which induces an increase of the cellulose concentration in the sample, the signal level (plateau) in the sample does not vary significantly. This results from the fact that the volume fraction of cellulose remains small, i.e. typically less than 10%, so that the impact of the presence of cellulose remains negligible on the signal. As a corollary, it is not possible to extract some reliable information about the evolution of the distribution of cellulose concentration in the sample.

In the next stage (between the dotted and the dashed line in Fig. 4), i.e. Regime B, the thickness of the sample does not change any more, meaning that no more shrinkage occurs. Instead the sample desaturates, first somewhat heterogeneously, with a gradient of concentration (first profiles after the dotted curve in Fig. 4), then homogeneously up to the end of this regime: the profiles evolve parallel to each other; more precisely, two of them are similar by a given factor of the NMR signal, which means that the concentration of water decreases homogeneously throughout the sample.

In the last stage, i.e. Regime C, after the dashed curve, the top edge of the profile seems to move progressively towards the left, as if some dry region was growing from the free surface of the sample (see Fig. 4). It is worth noting that at the same time the level of the profile below this apparent dry region goes on decreasing, indicating that the material goes on desaturating homogeneously in the lower part of the sample. This process (dry front and desaturation below) continues until complete disappearance of the signal.

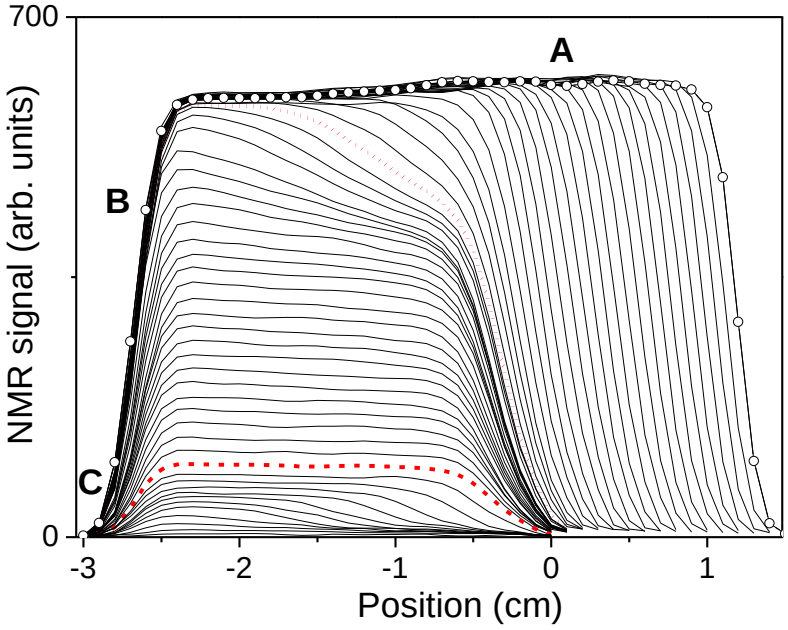

Fig. 4: Successive NMR water amount profiles (from top to bottom) along sample axis at different times (time interval 5 h) during drying of a cellulose paste. Transition to regime B at 124 h (red dotted line); transition to regime C at 248 h (red dashed line). The dry air

flux is imposed along the sample top. For the first profile we also plot the data points (corresponding to NMR signal in a cross-sectional layer) to illustrate the resolution of the measurement

Discussion

Regime A

In this regime the extraction of water due to evaporation along the free surface causes a shrinkage of the sample. The only possible force at the origin of such an effect is the Laplace pressure induced by the formation of liquid menisci around the sample top and resulting from water extraction. Menisci formed in this way have a characteristic radius of the order of half the pore size. This induces a Laplace pressure in the liquid, which acts on the fiber matrix and tends to shrink it (to reduce the area of the menisci). We thus can estimate the capillary stress as $2\gamma/R$ in which R is the typical pore radius in the network and $\gamma = 0.07\ \mathrm{N\ m^{-1}}$ the surface tension of water.

Since the fibers, which exhibit a very large aspect ratio, are entangled (even if they are only slightly deformed), the characteristic length (a) of fiber portion between two successive cross points with other fibers approximately corresponds to the pore size. By considering it corresponds to the radius of virtual spheres occupying the whole space (in disordered packing, i.e. at an apparent concentration of 62%), it is possible to estimate the variations of a with the solid fraction. Indeed, under these conditions the effective volume fraction of the cellulose is equal to the maximum packing fraction of these spheres times the fiber portion to sphere volume ratio, i.e. $\phi \approx 0.62 \times \left(a\pi b^2\right)/\left(4\pi a^3/3\right)$, where $b \approx 10\,\mu\mathrm{m}$ is the typical fiber radius. Note that taking into account the confined water in the fiber would induce a significant increase (see below) of b which, considering that the sample volume does not change significantly (see below), would induce approximately an increase of ϕ by a factor b^2, which leads to the same result: $a \approx 0.68 b \phi^{-0.5}$. This expression predicts that, for the initial solid fraction, $a \approx 30\,\mu\mathrm{m}$ and varies slowly when the concentration increases. The capillary stress which tends to contract the sample writes $4\gamma/a$, which is rather large but slowly varies with the concentration (see Fig. 5).

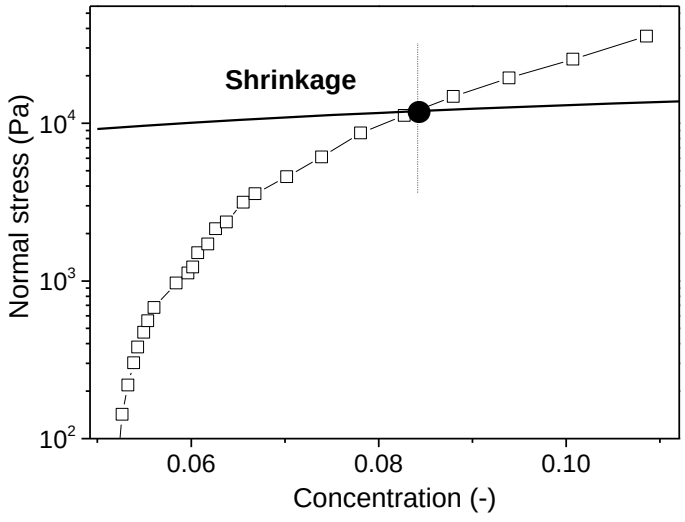

Fig. 5: Normal stress vs concentration (open squares) for the dry cellulose paste during a compression test (see Section Materials and Procedures), and estimation (see text) of the capillary stress for each concentration (continuous line). The dotted line marks the end of shrinkage; it is situated at the point of intersection of the two curves

On another side the resistance of the structure to shrinkage can be estimated from the force associated with the network compression in our test with dry cellulose packing (see Fig. 5). We observe that this force rapidly increases from low values with the concentration. Initially it is thus much smaller than the capillary stress, so that we expect that the first menisci resulting from water extraction will easily induce sample shrinkage. Then, as long the concentration increases the normal stress needed to reach this concentration increases, so that for some critical concentration value the capillary stress is insufficient to further induce compression, this corresponds to the point of intersection of the two curves in Fig. 4. Beyond that point the sample will essentially keep its shape and progressively desaturate. Here we find a critical concentration around 8.5%, which is close to the value (9.2%) found for the transition between Regimes A and B from MRI measurements.

As long as this shrinkage acts the liquid distribution around the free surface remains the same, which explains that the rate of drying remains constant (see below). Indeed, under these conditions the gradient in the vapor distribution around the free surface remains constant, which induces the same rate of vapor diffusion (Lehmann and Or 2013).

Regime B

In this regime, since the sample does not shrink anymore, the extraction of water necessarily induces a desaturation of the porous network. The initial volume fraction of cellulose in this regime is now 9.2%. We describe the water content through the saturation ψ, the liquid to pore volume fraction. During some initial stage the ψ decrease propagates downwards, which explains the gradient in the water profile observed at the beginning of Regime B (see Fig. 3). Then some slight gradient in water content remains but the profiles are essentially uniform and progress parallel to each other. This is the typical effect observed in simple porous media such as bead packings in a wide range of pore sizes (Thiery et al. 2017), which results from a capillary balance in the liquid network throughout the sample. For a fixed (i.e. non-shrinking) porous network initially filled by a wetting liquid the Laplace pressure increases when the saturation decreases, since the radius of the menisci decreases when the liquid films coating the structure get thinner. Some gradient of saturation in the sample then induces a flow from the more concentrated regions to the less concentrated ones, which has time to homogenize the concentration throughout the sample if the evaporation from the free surface is sufficiently slow.

As a consequence the drying in this regime takes the form of a liquid flow towards the free surface of the sample. Note that in this case vapor diffusion throughout the structure does not play a significant role because, as long as the air inside the sample is surrounded by liquid patches, the relative humidity inside the porous structure remains close to 100%. It follows that there is no gradient of RH along the sample length, and thus no vapor diffusion. This effect was for example demonstrated in a thin channel close on one side (see Keita et al., 2016 b): as long as there remains a continuous liquid film along the walls the RH is equal to 100% all along the channel and the liquid is drained towards the sample exit where it evaporates.

Moreover, as long the liquid patches are sufficiently close to each other, the relative humidity just above the free surface remains maximum, which ensures a constant rate of drying (Lehmann and Or 2013) and explains our observation (see Fig. 4).

Note that in this frame it is assumed that gravity is negligible. Actually, the impact of gravity may be appreciated by comparing the typical capillary stress in the partially saturated sample, i.e. $2\gamma/R$, to the characteristic stress due to gravity, i.e. $\rho g H$, with ρ the liquid density, H the sample thickness and g the gravity. In all our tests the ratio between the capillary stress and the gravity stress is much larger than 1, indicating that gravity effects are negligible.

Regime C

In this regime a new phenomenon occurs: an apparently dry region progresses downwards while the saturation goes on decreasing homogeneously in the rest of the sample (see Fig. 4). The saturation at which this effect starts to develop can be computed by dividing the amount of water at that time to the amount of water at the beginning of regime B, i.e. when the solid porous structure is fixed (at least for Regime B). We find a critical saturation of 18 %, which is in the order of the values found for bead packings with similar pore size (Thiery et al. 2013).

Such a dry front develops because, in contrast with the situation in Regime B, now the rate at which the water is extracted from the sample top is too large with regards to the rate at which it can flow for re-equilibrating the saturation due to capillary effects (see e.g. Coussot 2000). Indeed, the flow rate of liquid transport driven by capillary effects decreases when the liquid film thickness decreases, i.e. when the saturation decreases.

However, here, we have so far left aside the question of water state, assuming that we were dealing with a single type of water, in the form of free water in relatively large pores. Actually, we can get some information on the pore sizes in which water is embedded from the distribution of NMR relaxation times. Essentially four peaks are visible (see Fig. 6). Considering the relative large T2 values to which they are associated, the two peaks on the right likely correspond to free water in the pores of the structure of fibers, which would thus contain two types of pores of different characteristic sizes. It must be emphasized that the relaxation times of these two peaks are rather close, so the pore sizes too. Also note that from such basic measurements and without knowing the NMR relaxivity of the medium, it is not possible to quantify further, in a straightforward way, the exact pore size and shape. However we can usefully compare these results with those obtained with hardwood, which is a material for which we can expect a value of relaxivity close to that of cellulose, since water lies in a similar structure. We find that the T2 values of these two peaks are larger than the T2 value (around 100 ms) for water in fibers, whose diameter is about 10 microns, and smaller than the T2 value for vessels (around 600 ms), whose diameter if about 100 microns (Penvern et al. 2020). This confirms that the pore size of water in this range corresponds to a few tens of microns, as described above.

The third peak is situated at much smaller T2 values, around 20 ms. This a priori corresponds to water situated in pore size of the order of one micron. To go on with our comparison with NMR measurements in hardwood, a peak at such a T2 value was attributed to water in the rays of poplar (Penvern et al. 2020). Indeed, it is situated above (in terms of T2 value) that associated with bound water and below that associated with free water in fibers which, from structure observations, exhibit a smaller surface to volume ratio than the rays. Moreover, the fact that it is associated with a peak clearly distinct from the others means that there are very limited exchanges between free water and this water type. This will be confirmed by the observation that the free water peak disappears first while the third peak remains intact. This leads us to suggest that this peak corresponds to some (free)

water situated between the macrofibrils of the cellulose fibers. The fourth peak (on the left) seems to be somewhat mobile. We have no explanation for this mobility. However, the low value of the corresponding relaxation time, i.e. between 1 and 10 ms, indicates that the corresponding water is more deeply embedded than the rest of water. This might correspond to either water between microfibrils or bound water. A further analysis of this water type is provided by O'Neill et al. (2017). Note that the corresponding fraction of water is anyway rather low, as it appears from Fig. 6, which is consistent with the assumption that it corresponds to bound water. Indeed, the fiber saturation point being equal to 10%, we here expect the fraction of bound water to be equal to 0.7% of the total initial water amount.

These results and our analysis are consistent with those of Felby et al. (2008). The three main types of water identified here also appear to correspond respectively to the three water types identified by DSC, namely the bulk or free water, the freezing bound or capillary water, and the non-freezing bound water (Burghoff and Pusch 1979; Yamauchi and Murakami 1991; Weise et al. 1996). Finally, in the present context we will not further elaborate on these aspects but simply retain that these two peaks on the left are associated with water much more confined than the water associated with the two other peaks, and we will call them altogether "confined water". We will thus not distinguish between the two last types of water contained in micronic or nanometric pore sizes distinguished by Topgaard and Söderman (2002).

As drying progresses the peaks evolve differently. First the two peaks on the right at the same time decrease and move to the left, while the third and fourth peaks remain more or less the same (see Fig. 6). Finally the peak on the right disappears while the second peak goes on decreasing and approaches the third peak.

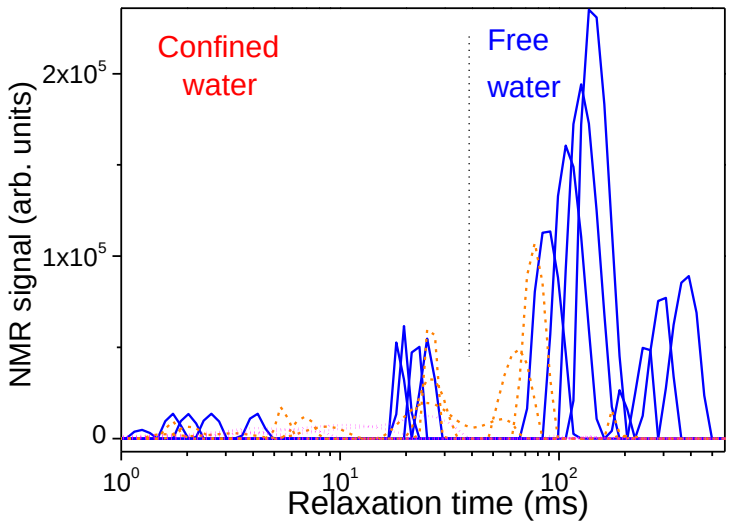

Fig. 6: Distributions of relaxation time for the whole cellulose paste sample during drying, at different times: (blue curves) 0, 50, 100, 150 h, (orange curves) 175, 200, 225 h, then every 12 h (magenta curves)

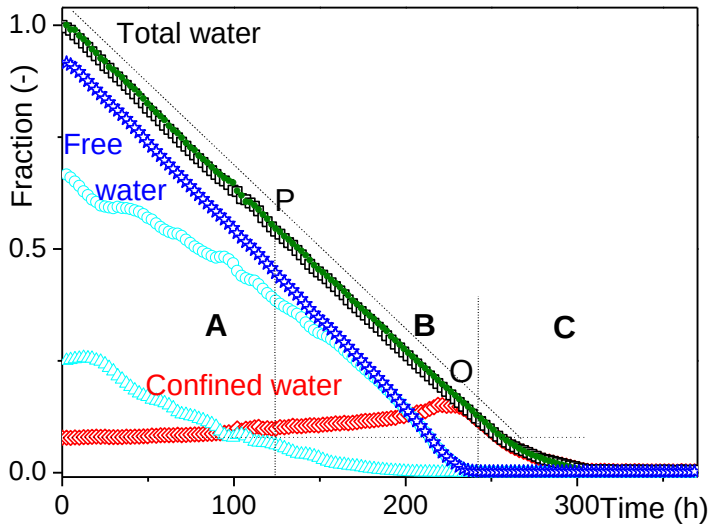

388

389 **Fig. 7**: Water fraction as a function of time for the different classes identified from the
390 distribution of relaxation times (see some of these distributions in Fig. 6): (triangles) first
391 peak on the right, (circles) second peak, (blue stars) total of these two peaks, i.e. free
392 water, (red diamonds) third and fourth peaks, i.e. confined water, (squares) total water.
393 The letters correspond to the different regimes identified in the text. The evolution of
394 the total fraction of water deduced from the integral of the water content profiles (see
395 Fig. 4) is also shown (small green filled circles)

396

397 We can follow more precisely the water amount associated with each class of water, by integrating
398 the distribution in the range associated with the corresponding type of water, i.e. below each peak.
399 The result of this integration should be proportional to the water mass in each class. The corresponding
400 fractions of water mass of each class are represented in Fig. 7. The total fraction (total water mass
401 divided by the initial value) is also computed from the integration of the successive profiles in time
402 shown in Fig. 4. The result is perfectly similar to the total fraction obtained from the T2 distribution
403 (see Fig.7), which confirms the validity of the technique.

404 We see that during Regime A (i.e. shrinkage regime) the two classes of free water progressively
405 disappear with a similar dynamics, while the confined water remains constant. Moreover, the
406 relaxation times of these two free water types decrease, i.e. the T-distribution is shifted towards lower
407 T2 values (see Fig. 6), which is consistent with the fact that during shrinkage the pore size progressively
408 decreases (Häggkvist et al. 1998). The amount of these two water classes and the corresponding
409 relaxation times (see above) go on evolving in a similar way in Regime B, during which no more
410 shrinkage occurs. This now reflects the fact that, as long as the saturation decreases in the porous
411 network, air occupies more space in the porosity, so that the liquid volumes form thinner films in
412 contact with the solid (cellulosic) structure, in which the water exhibits a smaller relaxation time than
413 in the filled pores. Importantly, as the T-distribution shifts towards lower values, the peak shapes
414 remain similar, i.e. they do not spread. This further proves that the desaturation is essentially
415 homogeneous throughout the sample, otherwise we would have some fraction of water still exhibiting
416 a relaxation time close to the initial one, and the right side of the peaks would remain attached (largest
417 T2 value) while the peaks spread towards lower T2 values.

Remarkably, in this regime, the apparent amount of confined water increases (see Fig. 7). We do not see any reason for which the effective amount of water between the macrofibrils would increase at that time since the maximum amount should have been absorbed rapidly after the cellulose has been put in contact with a large amount of water. More likely, here, as long as the porous medium desaturates, leading to a complex liquid network wetting the solid structure, some thin liquid films, say of micrometric thickness, form along some portions of the fiber surfaces, connecting liquid patches of much larger volumes (which ensures the bulk water transport towards the free surface, and thus ensures a constant drying rate). These liquid films exhibit a small relaxation time, of the order of that of the (main) confined water, so that they appear as confined water in our measurements. As desaturation progresses, more liquid films are formed and finally there remains (point O) only such liquid films in addition to confined water. From that point, the confined water and water in liquid films will progressively disappear in an indistinguishable manner.

Although we have no definite evidence it is likely that during regime B till point O the confined water amount remains constant. The situation is less clear beyond that point: the thin water films coating the external surface of the fibers and the thin water layers between macrofibrils might behave in a similar way. It is remarkable that during the period between point O and the beginning of regime C the drying rate (associated with total water evaporation) remains constant (see Fig. 7) and the water content distribution remains homogeneous (see Fig. 4).

We can have further information about the time at which the confined water starts disappearing from a more thorough look at the sample size evolution. Indeed, the extraction of this confined water should induce a contraction of the fiber, which should induce a contraction of the structure. However, the shrinkage of the sample structure based on a network of fibers in contact, and resulting from fiber shrinkage, depends on the distribution of fiber orientations and on the detailed shrinkage characteristics of the fibers (in their longitudinal and radial directions). According to our assumption of fiber shrinkage due to water penetration between macrofibrils it is natural to consider that they essentially shrink radially, i.e. longitudinal shrinkage is negligible. Then, the fiber network is a priori made of fibers in any direction and in contact. Along some direction, the average amount of cellulose fibers being equal to their volume fraction, the maximum shrinkage of the network is obtained if along this direction we only find fiber radial cross-sections (which is not possible from a strict point of view, as we need some fibers oriented along their longitudinal direction). In this ideal case, the sample shrinkage is equal to the loss of volume of the fibers relatively to the sample volume. Here the fraction of confined water, with regards to the sample volume, at the beginning of regime B (point P in Fig. 7) is found from the ratio of the confined water volume (1.1 cm3) to the sample volume (equal to the total water volume (6.6 cm3) plus the cellulose volume (0.67 cm3)), which gives 15%. So, according to the above reasoning, when the confined water is extracted, we expect a maximum shrinkage of 15% of the sample volume.

Now using the raw data associated with the 2D images we can determine the exact position of the small water container in time (see Fig. 8). We see that, apart from some slight discrepancy at the beginning of the test (due to the fact that it slightly sinks) the container follows exactly the water profile, which corresponds to the shrinkage regime (A), then it remains constant, which exactly corresponds to the desaturation regime (B). Interestingly, in Regime C, it starts again decreasing. This process is certainly due to the disappearance of confined water and we deduce that confined water disappears mainly in regime C. As a corollary, we can consider that only confined water remains in Regime C. The corresponding shrinkage is about 10% of the sample volume, which is below but still in the order of the maximum expected shrinkage from above calculations based on the extraction of confined water from fibers in a particular structure.

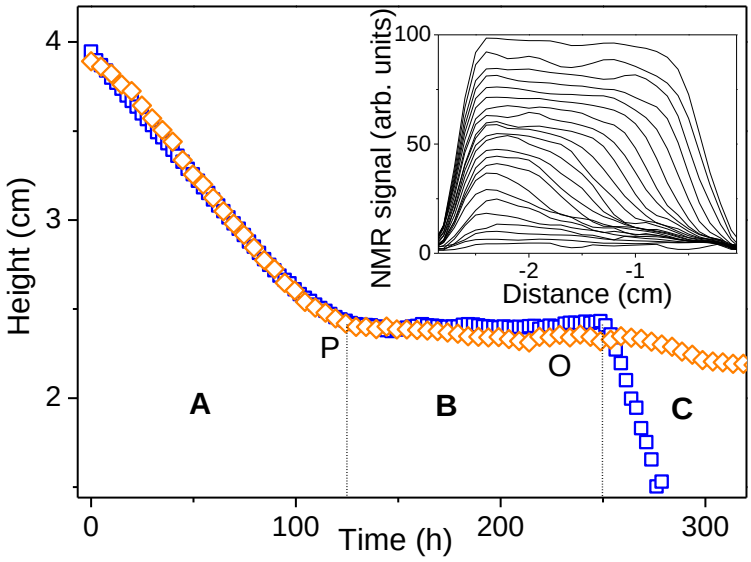

Fig. 8: Position of the feet of the small water tripod container (orange diamonds) and position of the apparent front of water (blue squares), i.e. mean position of the frontal part of the water profile, as a function of time. The inset shows the water content profiles during regime C: (from top to bottom) every 2.5 h from 248 h after the beginning of the drying test

From above measurements we can also estimate the shrinkage of cellulose fibers. The volume of cellulose being 0.67 cm3 and that of confined water 1.1 cm3, we deduce that the fiber volume should turn from 1.77 to 0.67 cm3, meaning that they individually shrink by a factor 2.6: their initial apparent volume is about 2.6 times their volume under dry conditions. In order to check this we observed the drying of a paste sample with ESEM. We did not quantify the drying progression but were able to observe the details of the paste structure when there remained essentially confined water. This is proved by the fact that we distinguish the shape of the cellulose fibers all along this period until full drying (see Fig. 9). Indeed, we can see that the shape of the fibers do not change during this period; if some water films were covering the fibers at the beginning (i.e. in Fig. 9a), except if they are extremely thin (a few nanometers) and then stabilized by the disjoining pressure, they could not follow exactly the shape of the fibers as the capillary equilibrium cannot be respected by simply covering such particles of complex shape with a film of given thickness.

From direct measurements on these images we find that on average the ratio between the diameter of the fibers in the first picture and that in the last picture is about 1.4, which means that the associated volume change is about 2. This value is lower than the expected one from above NMR measurements (i.e. 2.6), but this may be due to the fact that here we do not control the exact state of the material, i.e. we do not know if Fig. 9a corresponds to the first point for which there remains only confined water or a point later. In any event, these observations confirm the large individual shrinkage of the fibers, which further supports our interpretation of the NMR data.

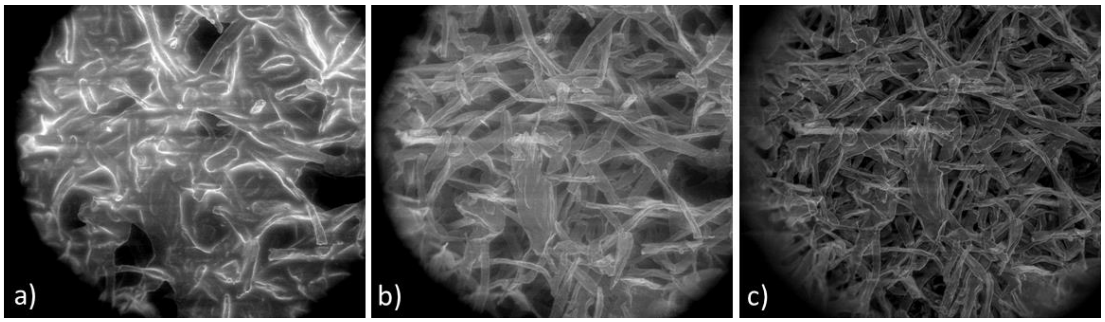

Fig. 9: Environmental scanning electron micrographs of a cellulose paste structure during drying

Under these conditions, if we assume that between O and regime C the free water films are drained homogeneously while the confined water remains fixed so that it does not play any role, the surprising result here is that usually in such a case, i.e. with thin films remaining along the pore walls, a dry front develops because the rate of transport driven by capillary effects is too low (Coussot 2000). The latter phenomenon explains the second period of drying necessary to remove the final liquid amount (typically for a saturation of 10 to 20% (Thiery et al. 2017). Here, if we consider the confined water fixed and thus a constitutive part of the solid porous structure, the saturation associated with the liquid films is 15%, in the range for which a dry front usually develops, whereas it appears that a dry front only develops from 248 hr of drying, when all these liquid films have disappeared.

This suggests that our assumption of a fixed confined water in the period starting from point O is wrong. There might be some simultaneous disappearance of both types of water. Instead we suggest that the films disappear first, without the development of a dry front, helped by confined water which plays a fundamental role in the process, by transporting the remaining water in the films towards the top surface of the sample. This effect is somewhat similar to that recently described in wood drying (Penvern et al. 2020). In this case the free water is partly dispersed in cavities inside the structure, with almost no connections, but a constant drying rate is observed as long as there remains bound water, which suggests that this bound water extracts free water from the interior of the sample and transports it towards the free surface.

The final extraction of confined water then would start only in regime C, leading to the development of a concentration gradient, looking almost like a dry front progressively invading the whole sample (see Fig. 8). It is worth emphasizing that during this process the water content below this dry region goes on decreasing homogeneously (see inset of Fig. 8). Such an effect results from some effect of re-equilibration of the water concentration in time, thanks to a transport process.

At this time we could assume that vapor diffusion throughout the structure could play a significant role in this water transport. However, the situation is finally similar to that for Regime B: the relative humidity inside the porous structure remains close to 100% as the air is surrounded by walls contained free water (even if this water somewhat confined, we are well above the Fiber Saturation Point). It follows that there is no gradient of RH along the sample length, and thus no vapor diffusion.

This is the definite evidence that this confined water can be transported through the sample. This leads to the surprising result that the water confined inside the cellulose fibers is able to be transported from fiber to fiber, through some connected hydraulic network.

Conclusion

We showed that during the drying of a cellulose paste all the bulk water, i.e. comprised between the fibers, is extracted first at a constant rate, while the drying rate remains constant. During this process the paste shrinks until capillary effects cannot induce further compression, then it homogeneously desaturates as long as gravity effects are negligible. In contrast with standard porous media, with a structure made of non-permeable solid material, the constant drying rate is maintained even when the bulk water content is very low. This is allowed thanks to the presence of free water confined inside the fibers, which can help transport the bulk water towards the sample free surface. This phenomenon exhibits some similarity to the effect observed: 1) for hardwood, in which bound water allows to transport free water almost enclosed in depth in the solid structure towards the sample free surface (Penvern et al. 2020), and 2) for model biporous systems (Lerouge et al. 2020) made of large pores dispersed in a matrix of small pores, in which the large pores are fully emptied first even in depth. In both cases a constant drying rate is observed all along these processes. In the case of the cellulose paste this extraction apparently relies on a continuous network of confined water throughout the structure, connected by fiber contacts.

Acknowledgments

The authors thank Joseph Lautru for his advice and availability regarding microscopic analysis.

Declarations:

Compliance with Ethical Standards:

- No conflict of interest
- This article does not contain any studies involving human participants performed by any of the authors.

Funding: This work was supported by the French Alternative Energies and Atomic Energy Commission and the EDDEM Project.

Availability of data and material: the data will be available on request.

Code availability: non applicable.

Authors' contributions: NBA, SR and BM carried out the NMR experiments, HD and XM carried out the macroscopic tests and material preparations; all authors discussed the data; BM, AG and PC wrote the paper.

References

Beaumont M, König J, Opietnik M, Potthast A, Rosenau T (2017) Drying of a cellulose II gel : effect of physical modification and redispersibility in water, Cellulose 24 :1199-1209. https://doi.org/10.1007/s10570-016-1166-9

Ben Abdelouahab N, Gossard A, Rodts S, Coasne B, Coussot P (2019) Convective drying of a porous medium with a paste cover, Eur Phys J E, 5:66. https://doi.org/10.1140/epje/i2019-11829-4

564 Bogdan M, Balcom BJ, Bremner TW, Armstrong RL (1995) Single-point imaging of partially dried,
565 hydrated white portland cement, J Magn Reson A, 116:266-269. DOI:10.1006/JMRA.1995.0019

566 Brownstein KR, Tarr CE (1977) Spin-Lattice relaxation in a system governed by diffusion, J Magn Reson,
567 26:17-24. https://doi.org/10.1016/0022-2364(77)90230-X

568 Burghoff HG, Pusch W (1979) Characterization of water structure in cellulose acetate membranes by
569 calorimetric measurements, J Applied Polymer Science, 23:473-484.
570 https://doi.org/10.1002/app.1979.070230217

571 Callaghan PT (1993) Principles of Nuclear Magnetic Resonance Microscopy, Oxford: Clarendon.

572 Coussot P (2000) Scaling approach of the convective drying of a porous medium, Eur Phys J B, 15:557
573 -566. https://doi.org/10.1007/s100510051160

574 Emid, S., & Creyghton, J. H. N. (1985) High resolution NMR imaging in solids, Physica B, 128:81-83.
575 https://doi.org/10.1016/0378-4363(85)90087-7

576 Faure P, Rodts S (2008) Proton NMR relaxation as a probe for setting cement pastes, Magn Reson
577 Imaging, 26:1183–1196. DOI: 10.1016/j.mri.2008.01.026

578 Felby C, Thygesen LG, Kristensen JB, Jorgensen H, Elder T (2008), Cellulose-water interactions during
579 enzymatic hydrolysis as studied by time domain NMR, Cellulose 15:703-710. DOI: 10.1007/s10570-
580 008-9222-8

581 Goavec M, Rodts S, Gaudefroy V, Coquil M, Keita E, Goyon J, Chateau X, Coussot P (2018)
582 Strengthening and drying rate of a drying emulsion layer, Soft Matter, 14:8612-8626. *DOI:*
583 10.1039/c8sm01490f

584 Häggkvist M, Li T-Q, Ödberg L (1998) Effects of drying and pressing on the pore structure in the
585 cellulose fibre wall studied by ^{1}H and ^{2}H NMR relaxation, Cellulose 5:33-49. DOI:
586 10.1023/A:1009212628778

587 Hubbe MA, Vendetti RA, Rojas OJ (2007) What happens to cellulosic fibers during papermaking and
588 recycling? A review, Bioresources, 2:739-788. DOI:10.15376/BIORES.2.4.739-788

589 Keita E, Kodger TE, Faure P, Rodts S, Weitz DA, Coussot P (2016 a) Water retention against drying
590 with soft-particle suspensions in porous media, Phys Rev E, 94:033104.
591 https://doi.org/10.1103/PhysRevE.94.033104

592 Keita E, Koehler SA, Faure P, Weitz DA, Coussot P (2016 b) Drying kinetics driven by the shape of the
593 air/water interface in a capillary channel, Eur Phys J E, 39:23. DOI: 10.1140/epje/i2016-16023-8

594 Korb JP (2018) Multiscale nuclear magnetic relaxation dispersion of complex liquids in bulk and
595 confinement, Progress in Nuclear Magnetic Resonance Spectroscopy, 104:12-55. DOI:
596 10.1016/j.pnmrs.2017.11.001

597 Lehmann P, Assouline S, Or D (2008) Characteristic lengths affecting evaporative drying of porous
598 media, Phys Rev E, 77:056309. https://doi.org/10.1103/PhysRevE.77.056309

599 Lehmann P, Or D (2013) Effect of wetness patchiness on evaporation dynamics from drying porous
600 surfaces, Water Resources Research, 49:8250. https://doi.org/10.1002/2013WR013737

601 Lerouge T, Maillet B, Courtier-Murias D, Grande D, Le Droumaguet B, Pitois O, Coussot P (2020) Drying
602 of a Compressible Biporous Material, Phys Rev Applied, 13:044061.
603 https://doi.org/10.1103/PhysRevApplied.13.044061

604 Lovikka VA, Khanjani P, Väisänen, Vuorinen T, Maloney T (2016) Porosity of wood pulp fibers in the
605 wet and highly open dry state, Microporous and Mesoporous Materials, 234 : 326-335.
606 https://doi.org/10.1016/j.micromeso.2016.07.032

607 O'Neill H, Pingali SV, Petridis L, He J, Mamontov E, Hing L, Urba, V, Evans B, Langan P, Smith JC,
608 Davison BH (2017) Dynamics of water bound to crystalline cellulose, Scientific reports, 7: 11840. DOI:
609 10.1038/s41598-017-12035-w

Park S, Venditti RA, Jameel H, Pawlak JJ (2006) Changes in pore size distribution during the drying of cellulose fibers as measured by differential scanning calorimetry, Carbohydrate Polymers 66:97-103. http://dx.doi.org/10.1016%2Fj.carbpol.2006.02.026

Peng Y, Gardner DJ, Han Y (2012) Drying cellulose nanofibrils : in search of a suitable method, Cellulose 24 :1199-1209. DOI: 10.12691/nnr-4-1-2

Penvern H, Zhou M, Maillet B, Courtier-Murias D, Scheel M, Perrin J, Weitkamp T, Bardet S, Caré S, Coussot P, How bound water regulates wood drying, Physical Review Applied (2020) 14:054051. https://doi.org/10.1103/PhysRevApplied.14.054051

Philippot S, Korb JP, Petit D, Zanni H (1998) Analysis of microporosity and setting of reactive powder concrete by proton nuclear relaxation, Magn Reson Imaging, 16:515–519. DOI: 10.1016/s0730-725x(98)00063-0

Posada P, Velasquez-Cock J, Gomez-Hoyos C, Serpa Guerra AM, Lyulin SV, Kenny JM, Ganan P, Castro C, Zuluaga R (2020) Drying and redispersion of plant cellulose nanofibers for industrial applications : a review, Cellulose 27:19. https://doi.org/10.1007/s10570-020-03348-7

Prado PJ, Balcom BJ, Beyea SD, Armstrong RL, Bremner TW (1997) Concrete thawing studied by single-point ramped imaging, Solid State Nuclear Magnetic Resonance, 10:1-8. https://doi.org/10.1016/S0926-2040(97)00071-4

Prat M (1993) Percolation model of drying under isothermal conditions in porous media, Int J Multiph Flow, 19:691-704. https://doi.org/10.1016/0301-9322(93)90096-D

Provencher SW (1982) A constrained regularization method for inverting data represented by linear algebraic or integral equations, Comput Phys Commun, 27:213–227. https://doi.org/10.1016/0010-4655(82)90173-4

Shokri N, Lehmann P, Or D (2009) Characteristic of evaporation from partially wettable porous media, Water Resources Research 45:W02415. https://doi.org/10.1029/2008WR007185

Sinquefield S, Ciesielski PN, Li K, Gardner DJ, Ozcan S (2020) Nanocellulose dewatering and drying : current state and future perspectives, ACS Sustainable Chem Eng 8:9601-9615. https://doi.org/10.1021/acssuschemeng.0c01797

Thiery J, Rodts S, Weitz DA, Coussot P (2017) Drying regimes in homogeneous porous media from macro- to nanoscale, Phys Rev Fluids, 2:074201. https://doi.org/10.1103/PhysRevFluids.2.074201

Topgaard D, Söderman O (2002) Changes of cellulose fiber wall structure during drying investigated using NMR self-diffusion and relaxation experiments, Cellulose 9 :139-147. https://doi.org/10.1023/A:1020158524621

Tsimpanogiannis IN, Yortsos YC, Poulou S, Kanellopoulos N, Stubos AK (1999) Scaling theory of drying in porous media, Phys Rev E, 59:4353‑4365. https://doi.org/10.1103/PhysRevE.59.4353

Van Brakel J (1980) Mass transfer in convective drying », in Advances in Drying (Hemisphere Publishing Corporation) 1:217‑267

Vergès-Belmin V, Heritage A, Bourgès A (2011) Powdered cellulose pultices in stone and wall painting conservation – Myths and realities, Studies in Conservation 56 :28-297. https://doi.org/10.1179/204705811X13159282692923

Weise U, Maloney T, Paulapuro H (1996) Quantification of water in different states of interaction with wood pulp fibres, Cellulose 3:189-202. https://doi.org/10.1007/BF02228801

Whittall KP, MacKay AL (1989) Quantitative interpretation of NMR relaxation data, J Magn Reson 84:134–152. https://doi.org/10.1016/0022-2364(89)90011-5

Yamauchi T, Murakami K (1991) Differential scanning calorimetry as an aid for investigating the wet state of pulp, J Pulp and Paper Science, 17:223-226

Yiotis AG, Salin D, Tajer ES, Yortsos YC (2012) Drying in porous media with gravity-stabilized fronts: Experimental results, Phys Rev E, 86:026310. https://doi.org/10.1103/PhysRevE.86.026310